Original Articles

Acupuncture and Herbal Medicine

Genome-wide analysis of electroacupuncture in restoring splicing regulation after myocardial ischemia-reperfusion injury

Wenchuan Qi[1,2,*,]Yida Wang[3], Sitthichock Vadphimai[4], Xiao Wang[1,2], Zixuan Yan[1], Jingwen Li[1], Chenghua Li[1], Jinqun Hu[1], Yu Liu[1], Jian Xiong[1], Ruirui Sun[1,2,*], Fanrong Liang[1,2,*]

[1]Chengdu University of Traditional Chinese Medicine, Chengdu, China; [2]Key Laboratory of Acupuncture for Senile Disease (Chengdu University of TCM), Ministry of Education, Chengdu, China; [3]Key Laboratory of BioResource and Eco-Environment of Ministry of Education, College of Life Science, Sichuan University, Chengdu, China; [4]School of Integrative Medicine, Mae Fah Luang University, Chiang Rai, Thailand

Abstract

Objective: Pre-mRNA alternative splicing (AS) is an important post-transcriptional regulation mechanism. The abnormal splicing of genes can lead to cardiovascular diseases. Acupuncture has been shown to alleviate myocardial ischemia-reperfusion injury (MIRI), but most studies have focused on the regulation of gene expression by acupuncture. Previously, we reported that electroacupuncture (EA) can relieve angina by regulating the AS of GABARG2; however, the genome-wide regulation of AS by EA remains unknown.

Methods: We explored the protective effects of EA on MIRI. We then studied the AS profiles retrieved from the previously submitted to Gene Expression Omnibus (GEO) database and analyzed the data using the replicate multivariate analysis of transcript splicing (rMATS) tool. Subsequently, we conducted validation experiments on splicing regulatory factors and their target genes modulated by EA, as identified through bioinformatics analysis.

Results: The results showed that EA at PC6 point could effectively alleviate MIRI. More than 200 differential alternative splicing events (ASEs) changed following MIRI. The differential ASEs underwent protein–protein interaction (PPI) network analysis, gene ontology (GO) enrichment, and pathway analysis, and were shown to be involved in distinct biological functions, especially in the maintenance of synaptic structure. Enrichment analysis also identified several pathways that are potentially associated with the progression of MIRI. Importantly, we identified critical ASEs and pathways that could be completely rescued by EA treatment. In the validation experiments, we found that AS of the key gene *CAMK2G*, associated with synaptic function, is regulated by the expression level of the MBNL1 protein modulated by EA.

Conclusions: Our results indicate that EA is not only an effective procedure to protect against MIRI by rescuing gene expression but also rescues abnormal ASEs. This study is a major contribution to a genome-wide comprehensive analysis of the regulation of AS by EA in MIRI.

Keywords: Alternative splicing, Alternative splicing events, Electroacupuncture, MIRI, rMATS

Graphical abstract: https://links.lww.com/AHM/A212

Introduction

Pre-mRNA alternative splicing (AS) is an important post-transcriptional regulatory process that is ubiquitous in eukaryotic organisms[1–3]. AS results in multiple mature mRNA splice variants that are translated into varying protein isoforms. With advances in high-throughput sequencing technology, data have shown that AS occurs in more than 95% of the human genes[4]. In post-transcriptional regulatory networks, AS is not only the major source of proteome diversity in humans but is also highly relevant to human diseases[5]. AS has been found to be a key step in gene regulation that affects nearly all aspects of myocardial development and function[6–7]. Previous studies have reported abnormal splicing of some gene transcripts that causes the occurrence and development of cardiovascular diseases[8–10]. The sodium channel gene, *SCN5A*, encodes the Na^+ channel subunit expressed in the human heart. Abnormal splicing of *SCN5A* would cause Brugada syndrome[11]. Kong et

Wenchuan Qi and Yida Wang contributed equally.

**Corresponding author. Wenchuan Qi, E-mail: qiwenchuan@cdutcm.edu.cn; Ruirui Sun, E-mail: sunruirui@cdutcm.edu.cn; Fanrong Liang, E-mail: acuresearch@126.com.*

How to cite this article: *Qi WC, Wang YD, Vadphimai S, Wang X, Yan ZX, Li JW, Li CH, Hu JQ, Liu Y, Xiong J, Sun RR, Liang FR. Genome-wide analysis of electroacupuncture in restoring splicing regulation after myocardial ischemia-reperfusion injury. Acupunct Herb Med 2026;6(1):91–104. doi: 10.1097/HM9.0000000000000188*

Received 05 June 2025 / Accepted 02 February 2026

al.[12] reported abnormalities in the AS of four sarcomere genes in dilated and ischemic cardiomyopathy that precede the onset of heart failure.

Accumulating thousands of years of clinical experience[13–16], acupuncture represents a traditional therapeutic system that has been used to treat heart diseases and pathological conditions. Many experimental studies have been conducted to investigate the effects of acupuncture on myocardial ischemia-reperfusion injury (MIRI) and have shown that it might have a multi-target and multi-channel synergetic regulatory effect. Acupuncture can effectively regulate oxygen-free radicals, vasoactive substances, myocardial ultrastructure, apoptosis, and nerve center in heart diseases[17–19]. Moreover, studies have confirmed that acupuncture can effectively intervene with the gene expression of signaling pathways in the death receptor and the mitochondrial and endoplasmic reticulum[20–21]. In addition to gene expression regulation, it would also be interesting to investigate whether acupuncture can participate in gene AS regulation. Our previous experimental study on the inhibition of angina pectoris revealed that electroacupuncture (EA) may participate in alleviating angina pectoris through AS of the inhibitory neurotransmitter *GABARG2* gene[22]. Recent advances in sequencing technologies have allowed the assessment of the role of AS in heart diseases[23]. The replicate multivariate analysis of transcript splicing (rMATS) algorithm is typically used to analyze transcriptomic profiles and identify alternative splicing events (ASEs)[24]. It quantifies the expression of variable splicing events in samples (with biological duplication) through the rMATS statistical model and then calculates the *P* value using the likelihood ratio test to express the difference between two groups of samples at the inclusion level. There are five AS modes that can be identified by rMATS: skipped exon (SE), retained intron (RI), mutually exclusion exons (MXE), alternative 5'splice site (A5SS), and alternative 3'splice site (A3SS)[24].

To identify the role of AS regulation in MIRI by acupuncture, we retrieved the RNA-seq raw data from the Gene Expression Omnibus (GEO) database using the accession number GSE61840[25]. We then analyzed ASEs using the rMATS software. Pearson's correlation was used to summarize the correlation between splicing factors and ASEs. Next, we constructed protein–protein interaction (PPI) networks to select the core modules of AS genes. The Database for Annotation, Visualization, and Integrated Discovery (DAVID v6.8) was used to perform gene ontology (GO) and Kyoto Encyclopedia of Genes and Genomes (KEGG) pathway analyses of the identified core modules. The underlying regulation of gene *CAMK2G* AS by EA treatment at the Neiguan (PC6) point was further analyzed. The results of this study may help further understand the potential mechanism of acupuncture in the treatment of MIRI by regulating AS.

Materials and methods

Experimental animals and ethics

Thirty specific pathogen free (SPF) -grade adult male Sprague Dawley (SD) rats, weighing 200 to 250 g, were provided by Chengdu Dashuo Experimental Animal Co., Ltd. (license number: SCXK Chuan-2020-030). The Animal Ethics Committee approval number is [2021132]. The feeding conditions are 12 hours of alternating light and dark, with a room temperature of 16°C to 28°C and a humidity of 40% to 70%. Before the experiment, adaptive feeding was carried out for 1 week, and standard feed and free drinking water were fed as a routine. The condition was good, the surrounding environment was fully familiar, and the activity was good. Subsequently, the formal experiment was initiated. All experimental procedures have been approved by the Animal Welfare and Ethics Committee of Chengdu University of Traditional Chinese Medicine, and conformed to the standards of the International Council for Experimental Animal Science and Animal Research: Reporting of In Vivo Experiments (ARRIVE) guidelines. This study conformed to the "Guide for the Care and Use of 114 Laboratory Animals" of the National Institutes of Health. The euthanasia methods utilized in our study were approved by the Committee on Care and Use of Laboratory Animal Resources and the Animal Care and Ethics Committee, ensuring adherence to ethical standards.

Experimental grouping

This experiment consisted of three groups: sham surgery group (SO), model group (ischemia/reperfusion [I/R]), and EA group at PC6, with 10 rats in each group. First, using the random number method, the rats were randomly divided into two groups: a sham surgery group of 10 rats and a modeling group of 20 rats. A myocardial ischemia-reperfusion model was replicated in the modeling group of rats, with a significant elevation of the ST segment of the electrocardiogram (ECG) or elevation of the T wave as a sign of successful coronary artery ligation for myocardial ischemia. After loosening the ligation of the coronary artery, a decrease of more than 1/2 of the ST segment of the ECG indicated successful construction of the MIRI model.

EA therapy

Seven days before modeling, rats in the EA group received EA daily for 20 minutes per session. PC6: Located in the middle of the medial part of the front lower limbs, 3 mm from the wrist transverse line, in the middle of the ulnar and radial sutures. Using an electric stimulator (Han's acupoint nerve stimulator from Nanjing, China, HANS-200), a frequency of 2/100 Hz and an intensity level of 1 mA to two 0.25 mm acupoints × 13 mm sterile acupuncture and moxibustion needle acupuncture and moxibustion needle (Suzhou Medical Supplies Factory, Jiangsu, China) were inserted into the point at a depth of 2 to 3 mm, lasting for 20 minutes.

Animal modeling

A rat model of myocardial ischemia-reperfusion was replicated using coronary artery ligation. The rats were anesthetized intraperitoneally, fixed in a supine position on the operating table, and connected to an ECG. Tracheal intubation was performed on the neck and the patient was connected to the ventilator. Make a 2 cm incision between the third and fourth ribs of the rats.

The subcutaneous tissue was separated layer-by-layer, the heart was exposed, sutures were used, the anterior descending branch was ligated, a knot was tied, and then covered with gauze moistened with physiological saline. The ventilator continues to supply oxygen for 30 minutes, opens the suture and knots, and completes reperfusion. Then, it is stitched layer-by-layer. After suturing, the ventilator was turned off, the sternum was pressed appropriately, and the rats were observed. After spontaneous breathing was stable, the skin of the area was sutured and the surgery was completed. The rats in the sham surgery group underwent the same surgical procedure as mentioned earlier, but only the heart was exposed without suturing the anterior descending branch of the coronary artery, and the chest for suturing[26]. During the process, a Lead II ECG was successively monitored and recorded under anesthesia from 30 minutes before the operation to 30 minutes after reperfusion. All 10 mice in the sham operation (SO) group survived. In the I/R group, four mice did not survive or were excluded because of unsuccessful modeling, leaving six mice for analysis. In the EA group, three mice were excluded because of unsuccessful modeling.

Detection indicators

Echocardiogram

All groups underwent cardiac ultrasound examination 24 hours after surgery, and the shaver removed hair from the left chest of the rat and exposed the skin within a range of approximately 3 cm × 3 cm. We used 2% isoflurane inhalation anesthesia with a ventilation rate set at 1.5 L/min. The anesthetized rat was fixed in a supine position on the operating table, and an appropriate amount of ultrasound coupling agent was applied to the left chest. Subsequently, a small animal color ultrasound imaging system (FUJIFILM Visuals, manufactured in Canada, Canada) was used for image acquisition. The left ventricular papillary muscle short-axis section of the tested rat was obtained near the left sternum, and the heart rate of the rats was maintained between 300 and 400 bpm. The left ventricular ejection fraction (LVEF) and fractional shortening (FS) were measured, and three consecutive cardiac cycles were detected, with the average value taken.

Histopathology analysis

The rats were euthanized for tissue examination on the day after the completion of cardiac ultrasound examination. The ischemic myocardium was fixed in neutral paraformaldehyde solution (4%) (Solarbio, Beijing, China) for tissue fixation. The heart tissue was cut into appropriate sections, washed, dehydrated, and embedded in tissue wax. The sample (4 μM thick) was sliced and stained with hematoxylin and eosin (H&E) (Solarbio) according to the manufacturer's instructions. To analyze the extent of damage, images were taken using a microscope (Nikon Corporation, Tokyo, Japan) to observe pathological changes in the slices.

Evans blue and TTC staining of the myocardial infarction area

The cardiac tissue was extracted and sectioned into slices of 1 mm thickness to assess the extent of infarction. The regions at risk and infarcted zones were delineated using a dual-staining technique employing Evans blue and 2,3,5-triphenyltetrazolium chloride staining (TTC). Analysis of the Evans blue-stained region (blue), TTC-stained region (red, indicating the area at risk), and TTC-non-stained region (pale, representing the infarcted myocardium) was conducted using ImageJ software version 1.53 (accessible at https://imagej.en.softonic.com/mac).

Myocardial enzyme spectrum detection

Blood was collected from the abdominal aorta of the rats and allowed to stand for 60 minutes. Serum was separated by centrifugation at 2,000 rpm for 10 minutes. The supernatant was collected, and the serum was transferred and packaged into corresponding numbered cryopreservation tubes. The blood was frozen in liquid nitrogen and stored in a –80°C ultra-low-temperature refrigerator for future use. The concentration was measured according to the instructions of the reagent kit (Wuhan Yilairuite Biotechnology Co., Ltd., Wuhan, Hubei, China), and an enzyme-linked immunosorbent assay (ELISA) was used to detect the concentrations of lactate dehydrogenase (LDH) and creatine kinase myocardial band (CK-MB) in rat serum.

Myocarditis factor detection

Rat hearts were harvested, ischemic myocardial tissue was cut, and transferred to correspondingly numbered cryopreservation tubes. The hearts were frozen in liquid nitrogen and stored at –80°C in an ultra-low-temperature refrigerator for future use. Approximately 50 mg of myocardial tissue was stored in a refrigerator at –80°C, placed in a grinder, and ground with a 9-fold homogenization medium. After grinding was completed, a pipette was used to transfer the grinding solution into a 2 mL centrifuge tube. After centrifugation at 3,000 to 4,000 rpm at 4°C for 10 minutes, the supernatant was extracted to prepare 10% tissue homogenate, operate, and measure the concentration using a reagent kit (Wuhan Yilairuite Biotechnology Co., Ltd.), and used to detect inflammatory factors such as interleukin (IL)-1β, IL-6, and tumor necrosis factor (TNF) in the myocardial tissue homogenate-α (TNF-α) level.

AS analysis

The software rMATS v4.0.1 was used to screen ASEs across different samples. First, we used the HISAT2 program (v2.1.0) to align the reads to the Rattus norvegicus reference sequence using default parameters, except for allowing for up to two mismatches. The aligned data were run on rMATS to perform AS analysis, and the SO group was treated as a control group. The AS events obtained were classified into five groups: SE, RI, A5SS, A3SS, and MXE. We then calculated the differential AS events with the thresholds of |Δ Percent

spliced in (PSI)| > 0.05, and the false discovery rate calculated from *P* value (FDR) <0.05. The PSI scores were estimated as follows: IncLevel Differences = IncLevel 1 – IncLevel 2, IncLevel = (IJC_SAMPLE/IncFormLen)/[(IJC_SAMPLE/IncFormLen) + (SJC_SAMPLE/SkipFormLen)], where IJC_SAMPLE_A denotes the inclusion junction counts for SAMPLE_A and SJC_SAMPLE_A represents the skipping junction counts for SAMPLE_A, *P* value represents the significance of the splicing difference between the two sample groups, IncLevel1 is the inclusion level for SAMPLE_1, and IncLevel2 is the inclusion level for SAMPLE_2. The ΔPSI value was calculated according to the ratio of the long form to the total present form (short form and long form) to characterize the inclusion of exons, differential splice-site choice, intron retention, etc. It is calculated as follows: ΔPSI (group1/group2) = PSI_group1 – PSI_group2; PSI upregulation: ΔPSI >0 indicates increased inclusion in the case of PSI downregulation. ΔPSI <0 indicates increased exclusion.

Construction of correlation network

The 71 human splicing factors were retrieved from the "SpliceAid-F" database (http://www.caspur.it/SpliceAidF)[27]. AS regulates gene expression and proteomic diversity, and the conservation of its factors is crucial for normal physiology and evolutionary stability. Splicing factors are highly conserved, suggesting that they have similar sequences and functions across species. Differentially expressed gene (DEGs) analysis was used to determine the significant splicing factors. DEGs were defined as relative transcription levels above the log fold change (FC) ≥|±2| and *q* value <0.05. In biological research, the Pearson correlation test is often used to assess the correlation between gene expression levels and other biological indicators. In this case, we investigated the relationship between the expression of splicing factor genes and PSI values of ASEs, |Rho| >0.95, *q* value <0.05. Correlation plots were generated using the Cytoscape software (v3.6.0).

PPI network and module identification

We used the String database v11.0 to determine the integrated functions of multiple genes and build the PPI network with the highest confidence (0.900) by providing the proteins in different groups as input. The PPI network was derived from human data, while ensuring the relevance of the analysis to our rat model through rigorous interpretation in the context of the study. Cytoscape v3.7.1 is an open-source software platform used for visualizing complex networks. The molecular complex detection MCODE plugin in Cytoscape v3.6.0, was used to identify the most densely connected region in the PPI based on the topology with the two k-cores, which could identify the core modules and hub genes in the PPI network.

GO enrichment and KEGG pathway analysis

Gene lists were submitted to DAVID v6.8 to perform GO enrichment and KEGG pathway analyses. *P* value <0.05 was used as a criterion to determine whether the enrichment analysis was statistically significant.

RT-PCR

Differentially expressed *CAMK2G* gene transcripts were analyzed using semiquantitative RT-PCR. Total RNA was reverse-transcribed to complementary DNA using the RevertAid RT Kit (Thermo Fisher Scientific, Waltham, Massachusetts, USA) following the manufacturer's protocol. The PCR conditions were as follows: initial denaturation at 94°C for 3 minutes, followed by 30 cycles at 95°C for 20 seconds, 55°C for 20 seconds, and 72°C for 20 seconds. The levels of two alternative transcript bands (inclusion/skipping) were evaluated by analyzing the PCR products using ImageJ software (version 1.36 b). The primers used were as follows.

MBNL1 Rat FORWARD: TGTGTCCGCAGCAACAACATC, REVERSE: GCTAATGACGTCGTCCTTACTC.
CAMK2G Rat: FORWARD: TGCCATCCTCACAACCATGC, REVERSE: ATTAGGTGCACGCTGGAACTC.

RNA Immunoprecipitation

Tissue lysates from the heart were combined with 1 mL IP buffer (25 mM Tris–Cl [pH 7.4], 150 mM NaCl, 0.5% NP-40, 0.5 mM dithiothreitol (DTT), and 1× complete protease inhibitors [Roche]) supplemented with 100 U/ml RNase Inhibitor (Thermo Fisher Scientific) and subjected to immunoprecipitation with 2-μg Mbnl1 antibody or IgG at 4°C overnight with rotation. The immunoprecipitants were digested with proteinase K (Thermo Fisher Scientific) and the immunoprecipitated RNA was recovered using TRIzol reagent (Thermo Fisher Scientific). cDNA was synthesized with random primers using a RevertAid RT Kit (Thermo Fisher Scientific) and subjected to RT-qPCR for CAMK2G transcripts. Primers used are as follows:

CAMK2G intron Forward (5'→3'): CTCACCACCAAGG ACTCAG CAMK2G intron Reverse (5'→3'): ATTGA GACCCCTTGTAACACTG

Western blotting

Protein samples were separated using 10% Sodium Dodecyl Sulfate – Polyacrylamide Gel Electrophoresis (SDS-PAGE) and transferred onto polyvinylidene difluoride membranes. Subsequently, the membranes were blocked with 5% skimmed milk powder in Phosphate Buffered Saline (PBS) before overnight incubation with primary antibodies at 4°C. Thereafter, the membranes were washed five times with PBS containing 0.1% Tween 20 and incubated with the secondary antibodies for 1 hour at room temperature. After secondary antibody incubation, the membranes were developed using an enhanced chemiluminescent (ECL) detection kit (MILLIPORE, Burlington, MA, USA), and the results were visualized using a Gel Imaging System (BioRad, USA). Antibodies against ZRANB2 (1:1,000) were purchased from Santa Cruz Biotechnology (Dallas, TX, USA). Mbnl1 antibody (1:1,000) was purchased from FineTest (Wuhan, China), and GAPDH (1:5,000) and

horseradish peroxidase-conjugated secondary antibodies were purchased from ProteinTech (Chicago, IL, USA).

Statistical analysis

Statistical analyses were conducted using either analysis of variance (ANOVA) or *t* tests, as specified in the Results section. In cases where ANOVA was applied, *post hoc* comparisons of means were performed using Tukey's test. Statistical significance was defined as a two-sided *P* value <0.05. Symbols indicating statistical significance are as follows: $^{**}P < 0.01$, $^{*}P < 0.05$.

Results

EA at PC6 protected the myocardium in MIRI

After 1 week of EA pretreatment (Figure 1A), EA significantly improved the typical echocardiogram findings due to I/R injury (Figure 1B), and the LVEF and FS values were significantly higher in the EA group than in the I/R group ($P < 0.01$) (Figure 1C). The pathological section results showed that the I/R group had distinct infarcted areas with more inflammatory cell infiltration than the SO group, and this was significantly alleviated in the EA group (Figure 1D). Compared to the SO group, serum LDH and CK-MB levels were significantly elevated in the I/R group, which is known to be the key indicator in the evaluation of myocardial injury, and this was significantly reversed by EA ($P < 0.01$) (Figure 1E). Myocardial IL-1β, IL-6, and TNF-α levels were significantly elevated in the I/R group compared with those in the SO group, but myocardial inflammation levels were decreased in the EA group (Figure 1F). The infarct area was measured by Evans blue/TTC staining. There was a significant difference in infarct size between the sham and I/R rats. EA treatment markedly reduced myocardial injury size (Figure 1G and H). The ECG records (Figure 1I and J) showed that the ST segments were visibly elevated after ischemia, and EA significantly reversed the S-T segment change. These results indicate that EA at PC6 could have a protective effect in rats with MIRI.

Identification of ASEs following MIRI in rats

To obtain ASEs after MIRI, we investigated the RNA-seq data (GSE61840) using the rMATS unpaired model (v4.0.1). The database contains data previously submitted by our collaborators, which have now undergone further in-depth analysis. First, we compared the occurrence of ASEs between the SO and I/R groups. In

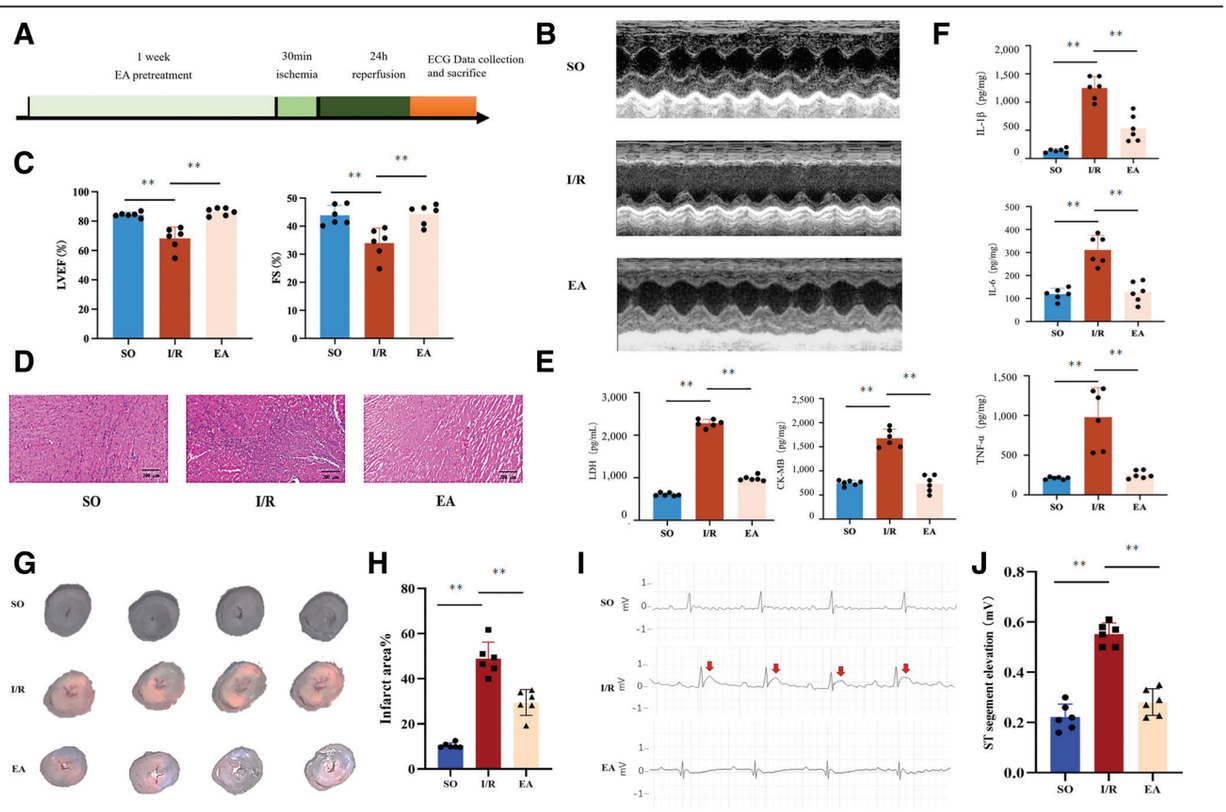

Figure 1. EA at PC6 protected the myocardium from MIRI. (A) Treatment and modeling timeline diagram. (B) Echocardiography; (C) LVEF and FS; (D) H&E staining of the heart; (E) LDH and CK-MB; (F) IL-1β, IL-6, and TNF-α in the SO, I/R, and EA groups. *n* = 6 per group. (G) Representative Evans blue/TTC staining of hearts harvested from the SO, I/R, and EA groups. (H) Infarct size percentage measured using ImageJ (*n* = 6 per group). (I) Representative ECG recordings, and the scale ranges from −1 to 1 mV. (J) Changes in rat ECG-ST (mV, A) of ECG in SO, I/R, EA groups, *n* = 6 per group. $^{*}P < 0.05$, $^{**}P < 0.01$. CK-MB: Creatine kinase myocardial band; EA: Electroacupuncture; ECG: Electrocardiogram; FS: Fractional shortening; H&E: Hematoxylin and eosin; I/H: Ischemia/reperfusion; IL: interleukin; LDH: Lactate dehydrogenase; LVEF: Left ventricular ejection fraction; MIRI: Myocardial ischemia-reperfusion injury; TNF-α: myocardial tissue homogenate-α; TTC: 2,3,5-triphenyltetrazolium chloride staining; SO: Sham operation.

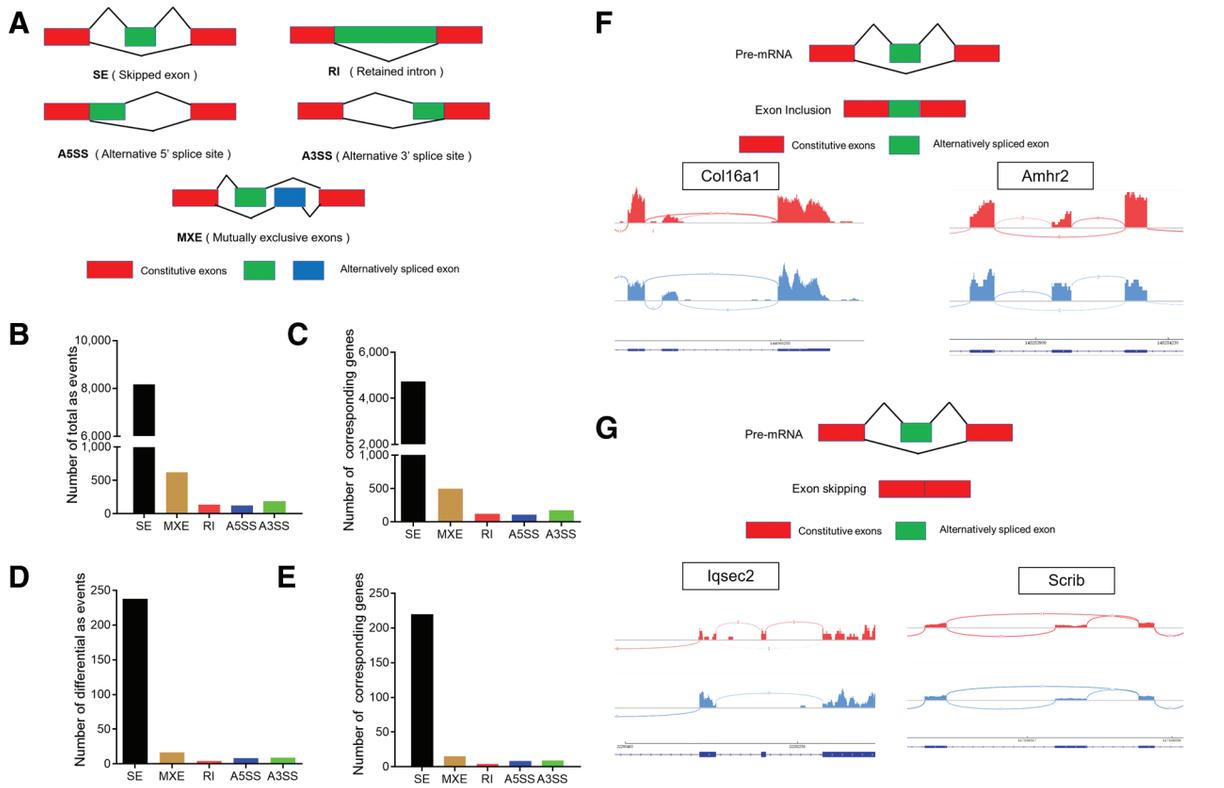

Figure 2. Identification of AS events in rat myocardial tissues after MIRI injury. (A) Five basic and generally recognized AS modes (A3SS, A5SS, MXE, RI, and SE). Red boxes represent constitutive exons, whereas green and blue boxes represent alternative exons. (B) The Number of AS events and (C) corresponding AS genes after MIRI injury in rats. AS events were classified as A3SS, A5SS, MXE, RI, and SE. (D) The number of differentials AS events and (E) corresponding AS genes after MIRI in rats. (F) A higher rate of inclusion exon events in Col16a1 and Amhr2 transcripts. (G) A higher rate of skipped exon events at the transcripts of Iqsec2 and Scrib. The tracks represent SO (red) and I/R (blue) samples. The number on the curved lines indicates continuous and differentially spliced exon–exon junction read counts. The x-axis depicts the genomic coordinates. For the sequencing peak diagrams, the red peaks indicate sequencing peaks of spliceosome exons formed after the inclusion of alternative exons, whereas the blue peaks represent sequencing peaks of exons resulting from exon skipping. A3SS: Alternative 3′SS; A5SS: Alternative 5′SS; AS: Alternative splicing; I/R: Ischemia/reperfusion; MIRI: Myocardial ischemia-reperfusion injury; MXE: mutually exclusive exons; RI: Retained introns; SE: Skipped exons.

this study, five basic and generally recognized AS modes were identified (A3SS, A5SS, MXE, RI, and SE), as shown in Figure 2A. Over 9,000 AS events were identified in >5,700 genes (Figure 2B and C). As shown in Figure 2B, genes with more than one AS type may be repeatedly calculated. Among the five major types of AS, SE was the most frequent after I/R injury, whereas A5SS was the least common AS pattern. For each AS type, we identified differential AS events with threshold[28] of $|\Delta PSI|$ >0.05, FDR <0.05, and *P* value <0.05 (Figure 2D and E). Among the 276 differential ASEs (DASEs), 238 were SE events, 17 were MXE events, four were RI events, nine were A3SS events, and eight were A5SS events.

rMATS sashimi plot software was used to visualize the rMATS analysis results. Figure 2F and G shows two randomly selected rMATS sashimi plots for exon inclusion events (Col16a1 and Amhr2) and SE events (Iqsec2 and Scrib) in the I/R group. The sashimi plot assay confirmed that exon inclusion cases were much more common in the I/R group than in the SO group. On the other hand, SE cases were much more prevalent in the I/R group than in the SO group. These results indicated that alternative gene splicing occurred following MIRI.

Network of splicing factor and ASEs in MIRI

Splicing factors are important executors of gene splicing; abnormal expression of splicing factors can lead to abnormal splicing events. Through DEGs analysis, we identified five splicing factors that were abnormally expressed after MIRI: Srp54a, Hnrnph2, Nova1, Zranb2, and Mbnl1 (Figure 3A). Interestingly, most of these five splicing factors have been previously reported to be related to the function of the nervous system[29–32]. We then conducted Pearson correlation analysis to determine the possible associations between splicing factors and ASEs and PSI values. The significant correlations are summarized in the network shown in Figure 3B. The expression of the five splicing factors was shown to be associated with 55 ASEs in the correlation network, among which 32 and 23 were significantly downregulated (green nodes) and upregulated (red nodes) ASEs, respectively. The splicing factor Nova1 was the factor most frequently associated with the ASEs.

We further constructed a PPI network of interactions between the DEGs and disease target proteins (Figure 3C). The PPI network generated by differential AS genes contained 323 nodes and 238 edges. Degree centrality (DC), betweenness centrality (BC), and closeness centrality (CC) values of the network were calculated using the

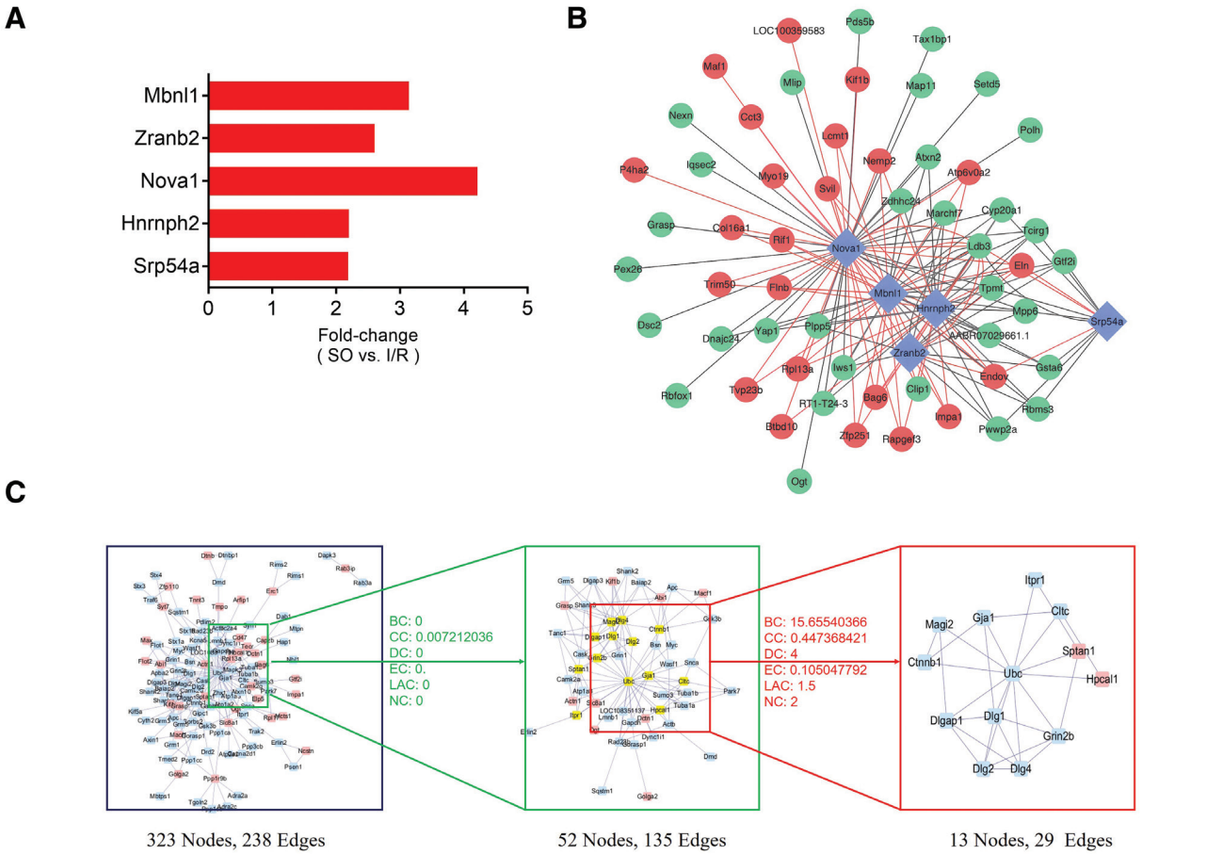

Figure 3. Correlation analysis between splicing factors and ASEs. (A) Splicing factor expression identified by DEGs. (B) Constructed network of splicing factors and splicing events. Blue nodes indicate splicing factors, green nodes represent downregulated splicing events, red nodes represent upregulated splicing events, red lines indicate positive correlations, and gray lines indicate negative correlations. (C) PPI consisting of 323 nodes with 238 edges. The first screening network comprised of 52 nodes and 135 edges. The core module consisted of 13 nodes with 29 edges. ASE: Alternative splicing events; BC: Betweenness centrality; CC: Closeness centrality; DC: Degree centrality; DEG: Differentially expressed gene; EC: Eigenvector centrality; I/R: Ischemia/reperfusion; LAC: local average connectivity-based method; NC: Network centrality; PPI: Protein–protein interaction; SO: Sham operation.

CytoNCA plugin and screened twice. The first screening network contained 52 nodes and 135 edges and the second contained 13 nodes and 29 edges. These 13 targets represented the core targets of the variable shear regulation mechanism of myocardial ischemia injury. The top 10 important targets were shown to be the following: Ubc, Dlg4, Dlg1, Dlgap1, Grin2b, Gja1, Dlg2, Magi2, Sptan1, and Hpcal1.

GO terms and KEGG pathway analysis of corresponding AS genes in MIRI

To provide more detailed information, we conducted GO analysis to explore the molecular function (MF), biological process (BP), and cellular component (CC) terms affected by the core module (Figure 4A). The top three BP terms were maintenance of the postsynaptic density structure, maintenance of the postsynaptic specialization structure, and maintenance of the synapse structure. Regarding the CC terms, the top terms were synaptic membrane, postsynaptic density, and asymmetric synapse. The top three MF terms were synaptic membrane, postsynaptic density, and asymmetric synapse. Functional grouping of identified DASEs may be important for postsynaptic signal integration, synaptic function, and maintenance. Meanwhile, RNA-binding protein-mediated AS has been reported to be essential for the functional specification of glutamatergic synapses in the mouse hippocampus[33]. The ultrastructure and biophysics of cardiac synapses underlie stable intercellular interaction[34]. Thus, the abnormal splicing of synapse-related genes may affect intercellular interactions in the heart. In addition, KEGG pathway analysis revealed that eight genes in glutamatergic synapses, eight in the Hippo signaling pathway, seven in Huntington disease, five in long-term potentiation, six in apoptosis, five in adherens junction, six in tight junction, five in gap junction, five in thyroid hormone signaling pathway, and four in endometrial cancer were differentially spliced in the I/R group compared with the SO group. KEGG pathway analysis showed that AS genes were associated with the cellular community in the heart (Figure 4B).

EA at PC6 pretreatment rescued abnormal ASEs

Previously, Huang et al.[25] have also confirmed the cardioprotective effects of EA in MIRI. They focused on the effects of EA on gene expression regulation. In this study, we investigated whether the regulation of AS by EA was involved in the cardioprotective process. Our results showed that compared with the I/R group, more than 8,000 ASEs pertaining to over 4,000 genes were

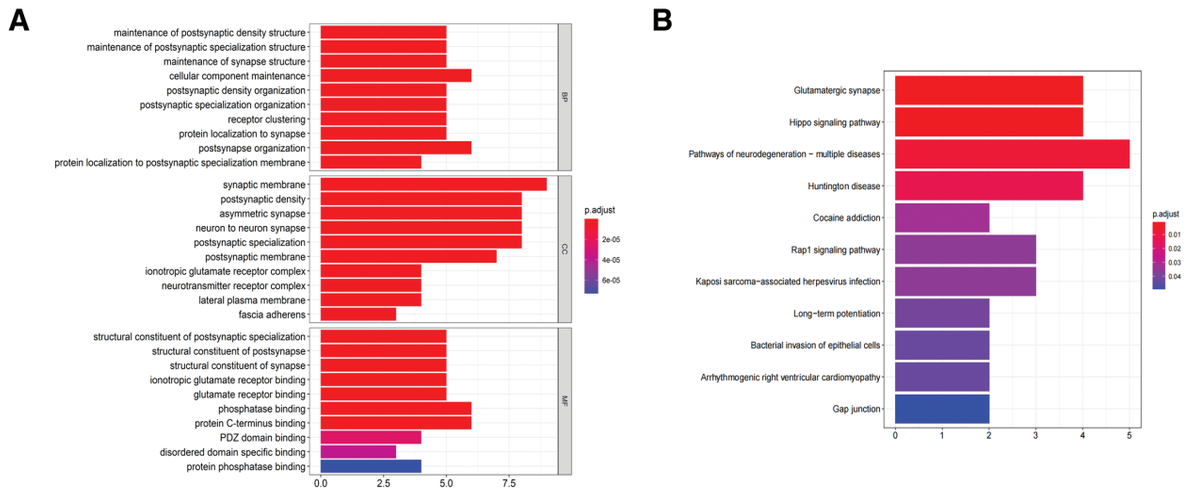

Figure 4. GO term and KEGG pathway analyses. (A) Analysis of biological processes, molecular functions, and cellular components. (B) Kyoto Encyclopedia of Genes and Genomes analysis of AS genes. AS: Alternative splicing; GO: Gene ontology; KEGG: Kyoto Encyclopedia of Genes and Genomes.

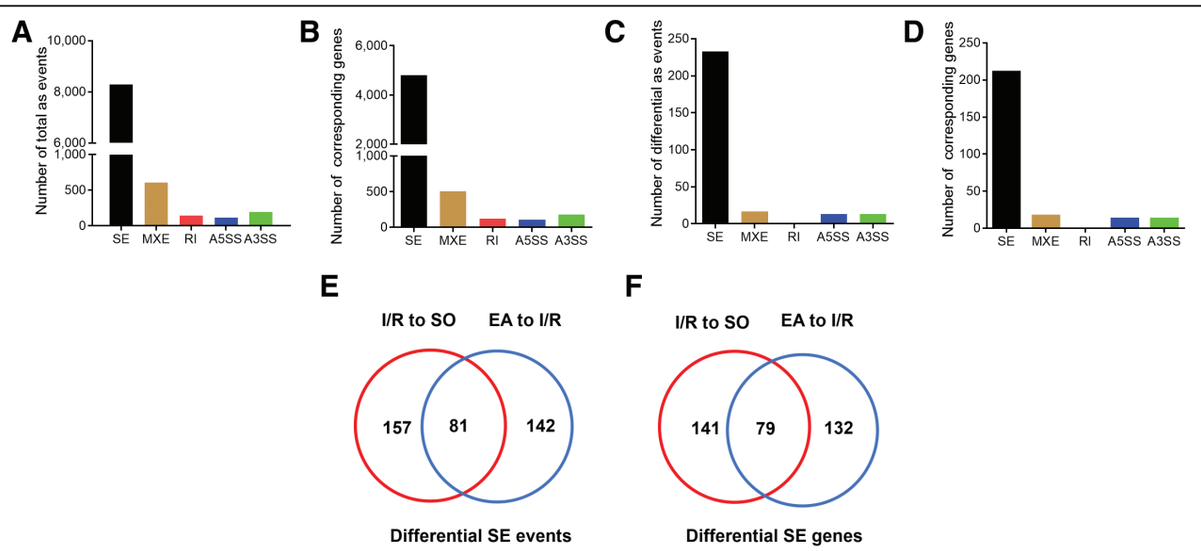

Figure 5. Identification of AS events in the EA group compared to the I/R group. (A) The total number of AS events and (B) the corresponding genes in the EA *vs.* I/R group. (C) Number of differential ASEs and (D) corresponding DAS genes in the EA *vs.* I/R group. AS events are classified into A3SS, A5SS, MXE, RI, and SE. (E) Number of overlapping differential SE events and (F) overlapping corresponding genes in the EA *vs.* I/R group. A3SS: Alternative 3′SS; A5SS: Alternative 5′SS; AS: Alternative splicing; ASE: Alternative splicing events; DAS: Differential ASE; DEA: Electroacupuncture; I/R: Ischemia/reperfusion; MXE: mutually exclusive exons; RI: Retained introns; SE: Skipped exons; SO: Sham operation.

observed in the EA group (Figure 5A and B), among which 276 events pertaining to 254 genes represented the differential ASEs. The 276 events included 223 SE, 17 MXE, 13 A3SS, and 13 A5SS events, and no RI events (Figure 5C and D). Additionally, SE events were the most frequent AS events. To further study the differences in AS between the different groups, we analyzed the overlap of SE events using Venn diagrams and compared the SO *vs.* I/R or EA *vs.* I/R groups. We identified 81 overlapping SE events in 79 genes (Figure 5E and F). Surprisingly, for these overlapping events, we noted that EA pretreatment rescued almost all I/R-induced changes in ASEs (80 of 81 differential ASEs were rescued). To provide more detailed information, the 20 overlapping SE differential ASEs with the lowest and highest IncLevel changes in the IR *versus* SO groups are listed in Supplementary Table S1, https://links.lww.com/AHM/A213. The IncLevel changes that resulted from EA pretreatment are included in Supplementary Table S2, https://links.lww.com/AHM/A213.

Pathway analysis of the EA rescued AS genes

I/R injury results in the abnormal regulation of hundreds of differential ASEs. Since the rats were subjected to EA pretreatment for 2 weeks, 80 differential ASEs were rescued. To investigate the potential pathways involved in this correction process, we utilized PPI network, GO terms, and KEGG pathway analysis. We constructed a PPI network of rescued AS genes, and the results showed that the PPI core network contained 22 nodes and 45 edges. The top 10 important targets were Ubc, Gja1, Hpcal1, Dlg1, Tuba1b, Tuba1a, Cltc,

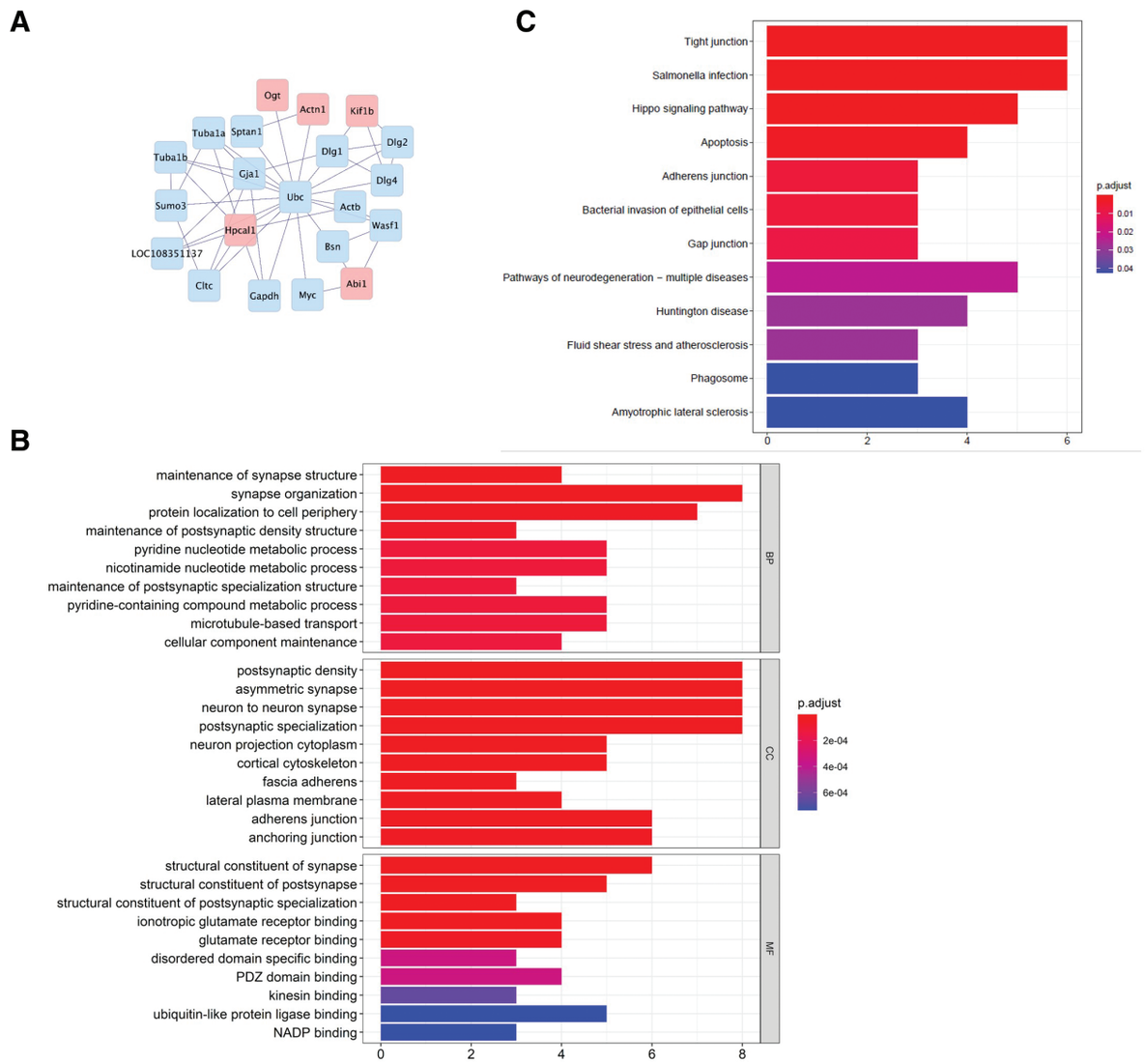

Figure 6. Enrichment analyses of the PPI network, biological process GO terms, and KEGG analysis of the EA-rescued AS events. (A) Core PPI network of the corresponding rescued AS genes. (B) Analysis of biological processes, molecular functions, and cellular components. (C) KEGG analysis of the rescued AS genes. AS: Alternative splicing; EA: Electroacupuncture; GO: Gene ontology; KEGG: Kyoto Encyclopedia of Genes and Genomes; PPI: Protein–protein interaction.

Sumo3, Gapdh, and LOC108351137 (Figure 6A). Next, we performed pathway analysis of the rescued core AS genes (Figure 6B). The top three BPs were maintenance of synapse structure, synapse organization, and protein localization to the cell periphery. Regarding CC terms, the top terms were postsynaptic density, asymmetric synapse, and neuron-to-neuron synapse. The top three MF terms were structural constituents of the synapse, structural constituents of the post-synapse, and structural constituents of postsynaptic specialization. Interestingly, comparing the I/R group with the SO group, we found that the rescued ASEs were also highly related to the maintenance of the structure and function of synapses, which may indicate that ASEs regulated by acupuncture are mainly involved in the maintenance of synaptic structure and function. The pathway analysis provided evidence that EA pretreatment could regulate some functional pathways, including tight junctions, Salmonella infection, the Hippo signaling pathway, apoptosis, adherent junctions, bacterial invasion of epithelial cells, gap junctions, pathways of neurodegeneration multiple diseases, Huntington disease, fluid shear stress and atherosclerosis, phagosomes, and amyotrophic lateral sclerosis. The results showed that most of the pathways regulated by EA pretreatment were similar to those of the IR *versus* SO KEGG pathways (Figure 6C). These results suggest that acupuncture pretreatment may rescue some key pathways by correcting AS events.

EA pretreatment corrects the abnormal ASEs through rescuing splicing factors

To further determine the possible mechanism underlying the effect of EA pretreatment on the accuracy of ASEs, we investigated whether EA could rescue the abnormally expressed splicing factors caused by MIRI. Interestingly, through DEG analysis, we found that most splicing

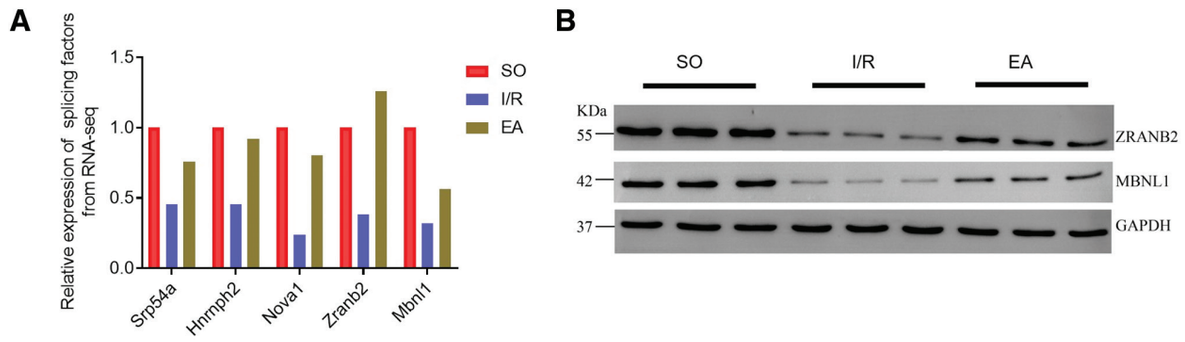

Figure 7. Relative expression of the five splicing factors. (A) Relative expression of splicing factors identified by DEGs. (B) WB detection of Zranb2 and Mbnl1 protein levels. DEG: Differentially expressed gene; EA: Electroacupuncture; I/R: Ischemia/reperfusion; SO: Sham operation; WB: western blot.

factors with abnormal expression caused by MIRI were rescued by EA pretreatment (Figure 7A). Therefore, we speculated that EA pretreatment can rescue splicing factors and correct abnormal ASEs. We assessed the changes in the protein levels of the two key AS factors. The results indicated that MIRI modeling led to a decrease in the expression of splicing factors Zranb2 and Mbnl1. However, after EA intervention, the protein expression levels were rescued (Figure 7B).

EA treatment ameliorates the AS of the CAMK2G gene

Calcium/calmodulin-dependent protein kinase II (CaMK2) is the most abundant protein in excitatory synapses, and is central to synaptic plasticity, learning, and memory. As shown in Figure 6B, AS of synapse-related genes is a key pathway in EA-mediated repair. By screening the recovered alternatively spliced genes listed in Supplementary Tables 1 and 2, https://links.lww.com/AHM/A213, we identified a key CaM-dependent gene, *CAMK2G*, which contains multiple splice variants and is involved in the development of various heart diseases. Figure 8A shows that exon 13 of this gene was an alternative exon. To determine whether EA treatment regulated this exon, we found that MIRI modeling led to the inclusion of exon 13, whereas this inclusion was reduced after acupuncture treatment (Figure 8B). According to predictions from the StarBase database (https://rnasysu.com/encori/), MBNL1 binds to the intronic region near exon 13 of this gene (Figure 8C). To determine whether EA treatment regulates MBNL1 expression and affects AS of the *CAMK2G* gene, we performed an RNA-IP assay to detect the binding of MBNL1 to the introns of this gene (Figure 8D). The results showed that MBNL1 indeed binds to the CAMK2G introns, and this binding was reduced after modeling, but was restored following EA treatment. Thus, we identified MBNL1 as a splicing factor regulated by acupuncture, which is involved in AS regulation of CAMK2G.

Discussion

This was a genome-wide comprehensive analysis to explore the involvement of EA in the regulation of AS in MIRI. First, we analyzed the effectiveness of EA in the treatment of MIRI. The results showed that EA effectively improved MIRI. Our study identified differential ASEs caused by MIRI, and differential SE mode appeared to be the most predominant AS in the I/R group. ASEs have been implicated in various pathways, including the maintenance of synaptic structures. By comparing I/R *versus* SO with EA *versus* I/R, we also found that among the 81 overlapping differential ASEs, 80 differential ASEs were rescued by EA pretreatment, while many of these corresponding AS genes were associated with the maintenance of the structure and function of synapses. By comparing the expression levels of splicing factors in the different groups, we found that some key splicing factors could be rescued by EA pretreatment. Furthermore, we experimentally verified that acupuncture correction of ASEs may be achieved by rescuing abnormal splicing factors (Figure 9).

RNA-seq can accurately detect gene expression and is widely used to evaluate ASEs in animal and plant genomes[35]. Acupuncture is widely accepted as an effective clinical therapy for several diseases. Clinical and experimental research has shown that acupuncture at PC6 has therapeutic effects on coronary heart disease (CHD), heart arrhythmias, and MIRI[36–38]. Acupuncture at PC6 can improve the symptoms of angina pectoris and palpitations, and enhance left ventricular function in CHD. Several molecular regulatory mechanisms have been gradually revealed to be active during acupuncture treatment of MIRI. However, whether acupuncture can participate in the treatment of heart disease by regulating the AS of genes remains unclear. In the current study, the preliminary findings showed that many ASEs have potential regulatory effects on MIRI. After analyzing the pathways involved in the corresponding AS genes, GO analysis showed that AS genes were enriched in BPs related to synapse formation and secretion. Previous studies have shown that cardiac synapses underlie stable intercellular interaction[39]. Sympathetic synapses exist in the heart, and the interaction between the nervous and cardiovascular systems is critical for determining the therapeutic potential of modulating autonomic tone in heart diseases[40]. Therefore, acupuncture may play a therapeutic role in heart diseases by adjusting the function

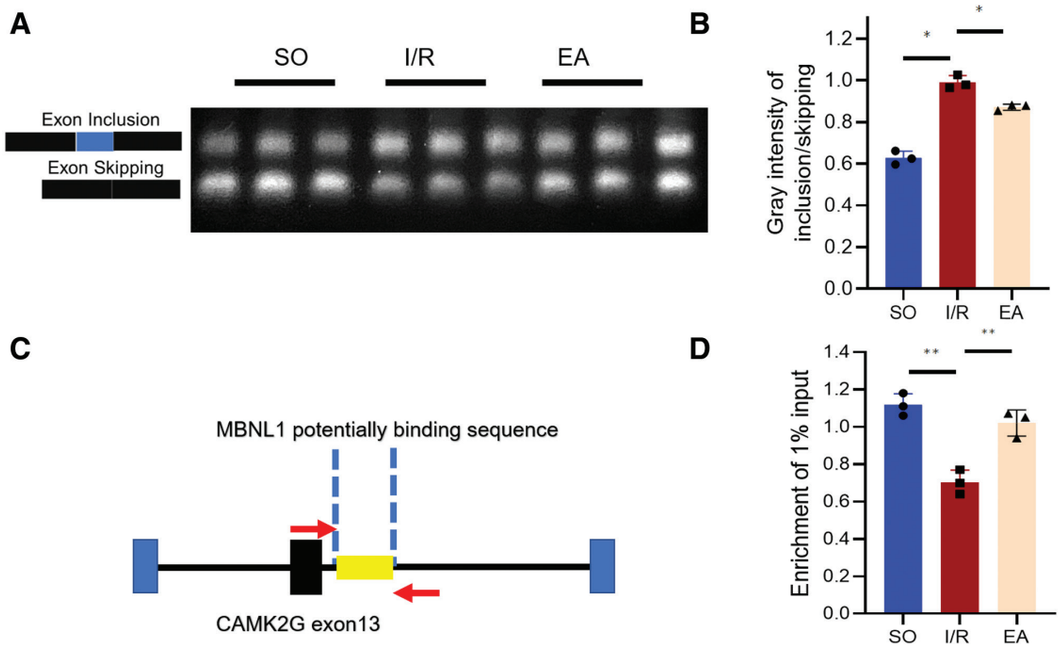

Figure 8. EA regulates the AS of CAMK2G through splicing factor MBNL1. (A) RT-PCR analysis of the AS pattern of CAMK2G cells. (B) Inclusion/skipping band intensity changes in the AS of CAMK2G across different groups. (C) Predicted binding of the splicing factor MBNL1 to the CAMK2G intron. (D) RNA-IP assay to detect the binding of MBNL1 to CAMK2G introns in different groups, $n = 3$. *$P < 0.05$, **$P < 0.01$. AS: Alternative splicing; EA: Electroacupuncture; I/R: Ischemia/reperfusion; RNA-IP: RNA immunoprecipitation; SO: Sham operation.

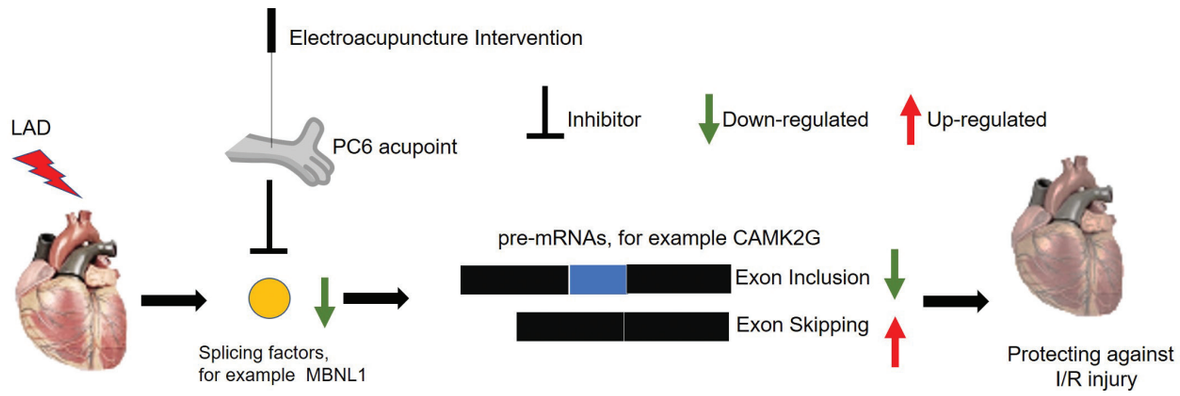

Figure 9. Proposed model for ameliorating dysregulation of AS through electroacupuncture at PC6. When myocardial ischemia-reperfusion occurs, more than 200 differential ASEs change following MIRI, as do splicing factors with abnormal expression caused by MIRI. This is similar to the splicing factor MBNL1, which leads to the disturbance of AS in some genes in myocardial tissue, such as CAMK2G, and causes myocardial tissue damage. Electroacupuncture intervention can restore the expression level of splicing factors, ameliorate dysregulation of AS, and participate in the repair of myocardial tissue. AS: Alternative splicing; ASEs: Alternative splicing events; I/R: Ischemia/reperfusion; MIRI: Myocardial ischemia-reperfusion injury.

of the sympathetic nerves[41–42]. Based on our results, we speculated that acupuncture may be involved in the maintenance of the function and structure of synapses by regulating AS. Our results also indicate that some corresponding AS genes are involved in key signaling pathways, including apoptosis, which aggravates and promotes the occurrence and progression of MIRI. Further research should be conducted to determine how these AS genes are involved in MIRI.

Splicing factors are involved in the splicing process. Therefore, changes in splicing factor expression can lead directly to abnormal splicing events. Previous studies have reported significant differences in the expression of splicing factors in heart diseases[6,43]. In this study, we constructed a potential regulatory network for the ASEs and splicing factors. Since we did not find any available splicing factor database for rats, the potential regulatory network of ASEs and splicing factors was constructed using a database of human splicing factors. However, using DEGs obtained from RNA-seq data, the expression of five of 71 splicing factors was significantly changed, including Srp54a, Hnrnph2, Nova1, Zranb2, and Mbnl1. In the nervous system, splicing factors are key regulatory elements. They regulate ASEs that participate in regulating synaptic function, synaptic plasticity, and the formation of neural circuits[44]. Srp54, also known as SFRS11, is a Tau exon 10 splicing repressor. The tau gene encodes a microtubule-associated protein that is critical for neuronal survival and function[29].

Heterogeneous nuclear ribonucleoprotein H2 (Hnrnph2) specifically interacts with the spliced RNA segment (exon 7) of Trf2 pre-mRNA[30]. Trf2 inhibition in rodents promotes neuronal differentiation[45]. Nova-1 regulates RNA splicing or metabolism of specific developing neurons and participates in RNA processing, synaptic transmission, and other biological functions[31]. MIRI decreased the expression of the splicing factor Nova1, which was rescued by EA treatment. Nova1 regulates the AS of GABRG2, specifically in exon 9, where an important phosphorylation site is present[22]. ZRANB2 is upregulated in glioma tissues and its knockdown inhibits proliferation, migration, invasion, and vasculogenic mimicry formation in glioma cells. Sequestration of the splicing factor MBNL1 results in the aberrant splicing of many genes in the DM1 skeletal muscle[32]. Additionally, we used Pearson correlation to determine associations with ASEs, which may play a crucial regulatory role in MIRI progression. Previous studies have shown that some splicing factors, such as Nova1[46] and Mbnl1[7], are associated with heart diseases. Moreover, EA pretreatment can rescue splicing factors with abnormal expression levels. This may be the reason why acupuncture can correct abnormal splicing events.

AS of CaMK2 plays a significant role in the development of diseases, particularly heart diseases[47]. CaMK2 can produce various splice variants through AS, which differ in protein structure, enzymatic activity, and substrate specificity[48]. These differences result in distinct functions and mechanisms of action of each splice variant within the cell. CaMK2δ is one of the primary isoforms in the heart, and its AS generates different isoforms that play distinct roles in heart diseases[49]. Some splice variants may exhibit increased enzymatic activity, leading to more severe outcomes under pathological conditions such as myocardial hypertrophy, heart failure, and arrhythmias[50–51]. In addition to heart disease, AS of CaMK2 may be involved in other diseases. For example, in the nervous system, overactivation of CaMK2 is closely associated with neurodegenerative diseases, such as Alzheimer disease[52]. Different splice variants may play different roles in these diseases, affecting neuronal function and survival. CaMK2 is a complex protein family comprising multiple isoforms including CaMK2α, CaMK2β, CaMK2γ (CaMK2G), and CaMK2δ[53]. However, the detailed mechanisms by which CaMK2γ directly participates in heart disease through AS have not been as extensively documented as those of CaMK2δ. Nonetheless, we can infer the potential mechanisms of CaMK2γ based on the general characteristics of the CaMK2 family and the role of AS in heart diseases. Different splice variants of CaMK2γ may possess varying enzymatic activities[54], affecting the regulation of signaling pathways within cardiac cells. In heart diseases, certain splice variants may exhibit increased enzymatic activity, leading to overactivation of signaling pathways and consequently promoting disease progression. These splice variants may recognize and bind to different substrate proteins that play crucial roles in the physiological and pathological processes of cardiac cells. Altering the substrate specificity of CaMK2γ *via* AS can influence the function and fate of the cardiac cells. Additionally, cellular localization of splice variants may be affected by AS[55]. This variation in localization can affect the interactions of CaMK2γ with other molecules within cardiac cells, thereby contributing to the development and progression of heart diseases. AS dysregulation of CAMK2γ (v1 loss) is a common feature of hypoxic oxygen-stable form of HIF1α (HIF-PPN), and ischemic myocardial infarction (MI), heart injury. HIF1 directly regulates CAMK2γ splicing, likely *via* Rbfox1 modulation, altering calcium signaling pathways[56]. Furthermore, CAMK2γ participates in cellular apoptosis and necrosis, and changes in its expression and activity are linked to cell death mechanisms such as apoptosis and necroptosis[57].

This study has several limitations: the rat MIRI model induced by coronary artery ligation fails to fully replicate the clinical complexity of MIRI, including comorbidities and individual differences, so the translational value of the findings requires verification in more clinically relevant models; due to the absence of a dedicated rat splicing factor database, reliance on human data for correlation analysis may introduce species-specific biases in the regulatory network, necessitating further validation with rat-specific resources; and while key ASEs (eg, CAMK2G) and their regulatory factors were identified and verified, the functional roles of most rescued ASEs in MIRI, such as their impact on synaptic function or myocardial cell physiology, remain unclear and require additional *in vitro* experiments for clarification. Future research should further explore the AS patterns of CaMK2γ, the functions and pathological significance of its different splice variants, and their specific connections and mechanisms in heart diseases. This will enhance our understanding of the mechanisms by which acupuncture treats heart diseases and provide new insights and methods for disease prevention and treatment. Besides, AS regulated by acupuncture should be further investigated to explore its potential role in the treatment of MIRI. In conclusion, this study provides information about genome-wide AS of EA treatment in MIRI, which can be used in future functional research.

Conclusion

This study explored EA at PC6's genome-wide role in AS during MIRI. EA pretreatment effectively alleviated MIRI, improving cardiac function and reducing infarct size. Genome-wide AS analysis found over 200 differential ASEs, with skipped exons predominant. EA rescued 80 of 81 abnormal ASEs. Mechanistically, it reversed key splicing factor expression and modulated CAMK2G splicing *via* MBNL1. This reveals EA's post-transcriptional regulation, offering a molecular basis for its MIRI therapy and new avenues for cardiovascular disease treatment.

Conflict of interest statement

Fanrong Liang is an editorial board ember of this journal, and other authors declare no conflict of interest.

Funding

This work was funded by the Natural Science Foundation of Sichuan Province (No. 2026NSFSC0636); the National Natural Science Foundation of China (No. 82205286); the Regional Cooperation Program of the National Natural Science Foundation of China (No. U21A20404); and the Program of China Scholarship Council (No. 202508510146).

Author contributions

Wenchuan Qi conceived the study design and experimental framework, performed most of the animal experiments, cell experiments, data analysis, and bioinformatics analysis, and drafted the manuscript. Yida Wang conducted cell experiments and bioinformatics analysis, and revised the manuscript critically for important intellectual content. Sitthichock Vadphimai, Xiao Wang, Zixuan Yan, Jingwen Li, Chenghua Li, Jian Xiong, Jinqun Hu, and Yu Liu assisted with animal experiments, cell experiments, and data analysis. Ruirui Sun and Fanrong Liang supervised the study, reviewed the manuscript, and approved the final version for publication. All authors have read and approved the final manuscript and agree to its submission.

Ethical approval of studies and informed consent

All experimental procedures have been approved by the animal welfare and Ethics Committee of Chengdu University of Traditional Chinese Medicine (2021132) and conform to the standards of the International Council for Experimental Animal Science.

Acknowledgments

We would like to thank Professor BingMei Zhu of West China Hospital of Sichuan University and her team for the RNA-seq data (GSE61840) submitted to the GEO database.

Data availability

The data that support the findings of this study are available from the corresponding author upon reasonable request.

Declaration of Generative AI in Scientific Writing

The authors declare that no generative artificial intelligence (AI) technologies were used in the conception, drafting, or revision of this manuscript. All work, including data analysis, interpretation, and writing, was performed solely by the human authors.

References

[1] Maniatis T, Tasic B. Alternative pre-mRNA splicing and proteome expansion in metazoans. *Nature* 2002;418:236–243.
[2] Wang ET, Sandberg R, Luo S, et al. Alternative isoform regulation in human tissue transcriptomes. *Nature* 2008;456:470–476.
[3] Johnson JM, Castle J, Garrett-Engele P, et al. Genome-wide survey of human alternative pre-mRNA splicing with exon junction microarrays. *Science* 2003;302:2141–2144.
[4] Pan Q, Shai O, Lee LJ, et al. Deep surveying of alternative splicing complexity in the human transcriptome by high-throughput sequencing. *Nat Genet* 2008;40:1413–1415.
[5] Stamm S, Ben-Ari S, Rafalska I, et al. Function of alternative splicing. *Gene* 2005;344:1–20.
[6] van den Hoogenhof MM, Pinto YM, Creemers EE. RNA splicing: regulation and dysregulation in the heart. *Circ Res* 2016;123:454–468.
[7] Kalsotra A, Xiao X, Ward AJ, et al. A postnatal switch of CELF and MBNL proteins reprograms alternative splicing in the developing heart. *Proc Natl Acad Sci U S A* 2008;105:20333–20338.
[8] Lara-Pezzi E, Gomez-Salinero J, Gatto A, et al. The alternative heart: impact of alternative splicing in heart disease. *J Cardiovasc Transl Res* 2013;6:945–955.
[9] Watanabe T, Kimura A, Kuroyanagi H. Alternative splicing regulator RBM20 and cardiomyopathy. *Front Mol Biosci* 2018;5:105.
[10] Dlamini Z, Tshidino SC, Hull R. Abnormalities in alternative splicing of apoptotic genes and cardiovascular diseases. *Int J Mol Sci* 2015;16:27171–27190.
[11] Wahbi K, Algalarrondo V, Becane HM, et al. Brugada syndrome and abnormal splicing of SCN5A in myotonic dystrophy type 1. *Arch Cardiovasc Dis* 2013;106:635–643.
[12] Kong SW, Hu YW, Ho JW, et al. Heart failure-associated changes in RNA splicing of sarcomere genes. *Circ Cardiovasc Genet* 2010;3:138–146.
[13] Ni YM, Frishman WH. Acupuncture and cardiovascular disease: focus on heart failure. *Cardiol Rev* 2018;26:93–98.
[14] Wang K, Tang M, Ouyang L, et al. Acupuncture for heart disease patients. *Eur J Prev Cardiol* 2018;25:1116.
[15] Zhao L, Li D, Zheng H, et al. Acupuncture as adjunctive therapy for chronic stable angina: a randomized clinical trial. *JAMA Intern Med* 2019;179:1388-1397.
[16] Lee H, Kim TH, Leem J. Acupuncture for heart failure: a systematic review of clinical studies. *Int J Cardiol* 2016;222:321–331.
[17] Yuan J, Wang JM, Cai Y, et al. Correlation between ischemic myocardial injury and inflammatory reaction, and anti-inflammatory effect of acupuncture. *Zhen Ci Yan Jiu* 2019;4:302–306.
[18] Li Y, Xiang Y, Liang J, et al. The mechanism and treatment strategies of GSDMD-mediated proptosis in myocardial infarction. *Acupunct Herb Med* 2024;4(3):295–305.
[19] Zhang XL, Huang W, Yang QQ, et al. Effect of electroacupuncture preconditioning on cell apoptosis mediated by mitochondrial reactive oxygen species in myocardial ischemia/reperfusion injury rats. *Zhen Ci Yan Jiu* 2020;12:961–967.
[20] Huang J, Yan J, Wang T, et al. Research progress on central autonomic nervous mechanism of acupuncture at Neiguan point in the treatment of atrial fibrillation. *Acupunct Herb Med* 2023;3(3):149–157.
[21] Zhang J, Zhu L, Li H, et al. Electroacupuncture pretreatment as a novel avenue to protect heart against ischemia and reperfusion injury. *Evid Based Complement Alternat Med* 2020;2020:9786482.
[22] Qi W, Fu H, Luo X, et al. Electroacupuncture at PC6 (Neiguan) attenuates angina pectoris in rats with myocardial ischemia-reperfusion injury through regulating the alternative splicing of the major inhibitory neurotransmitter receptor GABRG2. *J Cardiovasc Transl Res* 2022;15(5):1176–1191.
[23] Jiang W, Chen L. Alternative splicing: human disease and quantitative analysis from high-throughput sequencing. *Comput Struct Biotechnol J* 2021;19:183–195.
[24] Shen S, Park JW, Lu ZX, et al. rMATS: robust and flexible detection of differential alternative splicing from replicate RNA-Seq data. *Proc Natl Acad Sci U S A* 2014;51:E5593–E5601.
[25] Huang Y, Lu SF, Hu CJ, et al. Electro-acupuncture at Neiguan pretreatment alters genome-wide gene expressions and protects rat myocardium against ischemia-reperfusion. *Molecules* 2014;19:16158–16178.
[26] Kane KA, Parratt JR, Williams FM. An investigation into the characteristics of reperfusion-induced arrhythmias in the anaesthetized rat and their susceptibility to antiarrhythmic agents. *Br J Pharmacol* 1984;82(2):349–357.
[27] Giulietti M, Piva F, D'Antonio M, et al. SpliceAid-F: a database of human splicing factors and their RNA-binding sites. *Nucleic Acids Res* 2013;41(Database issue):D125–D131.
[28] Van Nostrand EL, Freese P, Pratt GA, et al. A large-scale binding and functional map of human RNA-binding proteins. *Nature* 2020;583:711–719.
[29] Wu JY, Kar A, Kuo D, et al. SRp54 (SFRS11), a regulator for tau exon 10 alternative splicing identified by an expression cloning strategy. *Mol Cell Biol* 2006;18:6739–6747.
[30] Grammatikakis I, Zhang P, Panda AC, et al. Alternative splicing of neuronal differentiation factor TRF2 regulated by HNRNPH1/H2. *Cell Rep* 2016;15:926–934.
[31] Zhou H, Mangelsdorf M, Liu J, et al. RNA-binding proteins in neurological diseases. *Sci China Life Sci* 2014;57:432–444.
[32] Furuta M, Kimura T, Nakamori M, et al. Macroscopic and microscopic diversity of missplicing in the central nervous system of patients with myotonic dystrophy type 1. *Neuroreport* 2018;29:235–240.
[33] Traunmuller L, Gomez AM, Nguyen TM, et al. Control of neuronal synapse specification by a highly dedicated alternative splicing program. *Science* 2016;352:982–986.
[34] Prando V, Da BF, Franzoso M, et al. Dynamics of neuroeffector coupling at cardiac sympathetic synapses. *J Physiol* 2075;2018(11):2055.
[35] Zhang H, He L, Cai L. Transcriptome sequencing: RNA-Seq. *Methods Mol Biol* 2018;175:15–27.

[36] Li Y, Barajas-Martinez H, Li B, et al. Comparative effectiveness of acupuncture and antiarrhythmic drugs for the prevention of cardiac arrhythmias: a systematic review and meta-analysis of randomized controlled trials. *Front Physiol* 2017;8:358.
[37] Ji C, Song F, Huang G, et al. The protective effects of acupoint gel embedding on rats with myocardial ischemia-reperfusion injury. *Life Sci* 2018;211:51–62.
[38] Meng J. The effects of acupuncture in treatment of coronary heart diseases. *J Tradit Chin Med* 2004;1:16–19.
[39] Pianca N, Di Bona A, Lazzeri E, et al. Cardiac sympathetic innervation network shapes the myocardium by locally controlling cardiomyocyte size through the cellular proteolytic machinery. *J Physiol* 2019;597:3639–3656.
[40] Lee SH, Kim DH. Synapses in the heart: sympathetic neurocardiac interaction modulates myocardial remodelling in healthy and diseased myocardium. *J Physiol* 2019;597:4441–4442.
[41] Middlekauff HR, Hui K, Yu JL, et al. Acupuncture inhibits sympathetic activation during mental stress in advanced heart failure patients. *J Card Fail* 2002;8:399–406.
[42] Middlekauff HR. Acupuncture in the treatment of heart failure. *Cardiol Rev* 2004;12:171–173.
[43] Zhu C, Chen Z, Guo W. Pre-mRNA mis-splicing of sarcomeric genes in heart failure. *Biochim Biophys Acta Mol Basis Dis* 2017;1863:2056–2063.
[44] Hermey G, Bluthgen N, Kuhl D. Neuronal activity-regulated alternative mRNA splicing. *Int J Biochem Cell Biol* 2017;91:184–193.
[45] Ovando-Roche P, Yu JS, Testori S, et al. TRF2-mediated stabilization of hREST4 is critical for the differentiation and maintenance of neural progenitors. *Stem Cells* 2014;32:2111–2122.
[46] Trujillo CA, Rice ES, Schaefer NK, et al. Reintroduction of the archaic variant of NOVA1 in cortical organoids alters neurodevelopment. *Science* 2021;371:eaax2537.
[47] Zhang W, Dong E, Zhang J, et al. CaMK2, "jack of all trades" in inflammation during cardiac ischemia/reperfusion injury. *J Mol Cell Cardiol* 2023;184:48–60.
[48] Sloutsky R, Stratton MM. Functional implications of CaMK2 alternative splicing. *Eur J Neurosci* 2021;54(8):6780–6794.
[49] Jia K, Cheng H, Ma W, et al. RNA Helicase DDX5 maintains cardiac function by regulating CaMK2δ alternative splicing. *Circulation* 2024;150:1121–1139.
[50] Duran J, Nickel L, Estrada M, et al. CaMK2δ splice variants in the healthy and diseased heart. *Front Cell Dev Biol* 2021;9:644630.
[51] Bell JR, Raaijmakers AJ, Curl CL, et al. Cardiac CaMK2δ splice variants exhibit target signaling specificity and confer sex-selective arrhythmogenic actions in the ischemic-reperfused heart. *Int J Cardiol* 2015;181:288–296.
[52] Yasuda R, Hayashi Y, Hell JW. CaMK2: a central molecular organizer of synaptic plasticity, learning and memory. *Nat Rev Neurosci* 2022;23(11):666–682.
[53] Cook SG, Bourke AM, O'Leary H, et al. Analysis of the CaMK2α and β splice-variant distribution among brain regions reveals isoform-specific differences in holoenzyme formation. *Sci Rep* 2018;8(1):5448.
[54] Kim K, Saneyoshi T, Hosokawa T, et al. Interplay of enzymatic and structural functions of CaMK2 in long-term potentiation. *J Neurochem* 2016;139(6):959–972.
[55] Liu J, Wang K, Liu X, et al. RBM24 controls cardiac QT interval through CaMK2δ splicing. *Cell Mol Life Sci* 2022;79(12):613.
[56] Williams AL, Walton CB, Pinell B, et al. Ischemic heart injury leads to HIF1-dependent differential splicing of CaMK2γ. *Sci Rep* 2021;11(1):13116.
[57] Chen B, Xie K, Zhang J, et al. Comprehensive analysis of mitochondrial dysfunction and necroptosis in intracranial aneurysms from the perspective of predictive, preventative, and personalized medicine. *Apoptosis* 2023;28(9–10):1452–1468.